Atmos. Chem. Phys. Discuss., 14, 27143–27193, 2014
www.atmos-chem-phys-discuss.net/14/27143/2014/
doi:10.5194/acpd-14-27143-2014
© Author(s) 2014. CC Attribution 3.0 License.

Atmospheric Chemistry and Physics Discussions

This discussion paper is/has been under review for the journal Atmospheric Chemistry and Physics (ACP). Please refer to the corresponding final paper in ACP if available.

Particle water and pH in the southeastern United States

H. Guo[1], L. Xu[2], A. Bougiatioti[2,8], K. M. Cerully[2,*], S. L. Capps[4], J. R. Hite[1], A. G. Carlton[5], S.-H. Lee[6], M. H. Bergin[1,3], N. L. Ng[1,2], A. Nenes[1,2,7], and R. J. Weber[1]

[1]School of Earth and Atmospheric Sciences, Georgia Institute of Technology, Atlanta, GA, USA
[2]School of Chemical and Biomolecular Engineering, Georgia Institute of Technology, Atlanta, GA, USA
[3]School of Civil & Environmental Engineering, Georgia Institute of Technology, Atlanta, GA, USA
[4]Office of Research and Development, United States Environmental Protection Agency, Research Triangle Park, NC, USA
[5]Department of Environmental Sciences, Rutgers University, New Brunswick, NJ, USA
[6]College of Public Health, Kent State University, Kent, Ohio, USA
[7]Foundation for Research and Technology, Hellas, Greece
[8]National Technical University of Athens, Athens, Greece
[*]now at: TSI, Inc., Shoreview, MN, USA

Received: 30 August 2014 – Accepted: 30 September 2014 – Published: 29 October 2014

Correspondence to: R. Weber (rodney.weber@eas.gatech.edu) and
A. Nenes (athanasios.nenes@gatech.edu)

Published by Copernicus Publications on behalf of the European Geosciences Union.

ACPD
14, 27143–27193, 2014

Abstract

Particle water and pH are predicted using thermodynamic modeling (with ISORROPIA-II), meteorological observations (RH, T), and gas/particle composition. A comprehensive uncertainty analysis is included and the model validated with ammonia partitioning. The method is applied to predict mass concentrations of particle water and related particle pH for ambient fine mode aerosols sampled in a relatively remote Alabama forest during the Southern Oxidant and Aerosol Study (SOAS) in summer, and at various sites in the southeastern US, during different seasons, as part of the Southeastern Center for Air Pollution and Epidemiology (SCAPE) study. Particle water and pH are closely linked; pH is a measure of the particle H^+ aqueous concentration, and so depends on both the presence of ions and amount of particle liquid water. Levels of particle water, in-turn, are determined through water uptake by both the ionic species and organic compounds. Particle ion balances, often used to infer pH, do not consider either the dissociation state of individual ions, nor particle liquid water levels and so do not necessarily correlate with particle pH. Thermodynamic calculations based on measured ion concentrations can predict both pH and liquid water, but do not consider contributions of organic species to liquid water and so may also be biased. In this study, contributions of both inorganic and organic fractions to aerosol liquid water were considered and predictions were in good agreement with measured liquid water based on differences in ambient and dry light scattering coefficients (prediction vs. measurement: slope = 0.91, intercept = 0.45 $\mu g\,m^{-3}$, $R = 0.87$). ISORROPIA-II predictions were evaluated by reproducing the observed gas-particle partitioning of NH_3. Based on this study, organic species on average contributed 35 % to the total water, with a substantially higher contribution (63 %) at night. The mean pH predicted in the Alabama forest (SOAS) was 0.94 ± 0.59 (median 0.93). Not including contributions of organic water has a minor effect on pH (changes pH by 0.15 to 0.23 units). pH diurnal trends followed liquid water and were driven mainly by variability in RH; in SOAS nighttime pH was near 1.5 and during day 0.5. pH ranged from 0.5 to 2 in summer and 1 to 3 in the win-

ACPD
14, 27143–27193, 2014

ter at other sites. The systematically low levels of predicted pH in the southeast may have important ramifications, such as significantly influencing acid-catalyzed reactions, gas-aerosol partitioning, and mobilization of redox metals and minerals.

1 Introduction

The concentration of the hydronium ion (H^+) in aqueous aerosols, or pH, is an important aerosol property that drives many processes related to particle composition and gas-aerosol partitioning (Jang et al., 2002; Meskhidze et al., 2003; Gao et al., 2004; Iinuma et al., 2004; Tolocka et al., 2004; Edney et al., 2005; Czoschke and Jang, 2006; Kleindienst et al., 2006; Surratt et al., 2007; Eddingsaas et al., 2010; Surratt et al., 2010). Despite its importance, measuring pH is not conserved during aerosol sampling because dilution makes its measurement highly challenging. For this reason, indirect proxies are used to represent particle acidity. The most common is an ion balance, the charge balance of measurable cations and anions (excluding the hydronium ion). Although correlated with an acidic (net negative balance) or alkaline (net positive balance) aerosol (Surratt et al., 2007; Tanner et al., 2009; Pathak et al., 2011; Yin et al., 2014), an ion balance cannot be used as a proxy for the aerosol concentration of H^+ in air (i.e., moles H^+ per volume of air, denoted hereafter as H^+_{air}). This is due to two factors, first, an ion balance assumes all ions are completely dissociated, but multiple forms are possible, depending on pH (e.g., sulfate can be in the form, of H_2SO_4, HSO_4^-, or SO_4^{2-}). A comparison between an ion balance-predicted H^+_{air} to that from the full analysis discussed below, for this data set, is shown in the Supplement. Secondly, pH depends on the particle liquid water content (LWC) (pH is the concentration of H^+ in an aqueous solution), which can vary considerably over the course of a day and between seasons and influence pH (Seinfeld and Pandis, 2006). Aerosol thermodynamic models, such as ISORROPIA-II (Nenes et al., 1998; Fountoukis and Nenes, 2007) and AIM (Clegg et al., 1998), are able to calculate LWC and particle pH, based on measurements or model predictions of aerosol species, temperature (T), and relative humidity

ACPD
14, 27143–27193, 2014

(RH) and offer a more rigorous approach to obtain the aerosol pH (Pye et al., 2013). ISORROPIA-II calculates the composition and phase state of an NH_4-SO_4-NO_3-Cl-Na-Ca-K-Mg-water inorganic aerosol in thermodynamic equilibrium with water vapor and gas phase precursors. The model has been tested with ambient data to predict acidic or basic compounds such as $NH_{3(g)}$, $NH_{4(p)}$, and $NO_{3(p)}$ (Meskhidze et al., 2003; Nowak et al., 2006; Fountoukis et al., 2009; Hennigan et al., 2014).

LWC is a function of RH, particle concentration and composition, and predicted to be the most abundant particle-phase species in the atmosphere, at least 2–3 times the total aerosol dry mass on a global average (Pilinis et al., 1995; Liao and Seinfeld, 2005). At 90 % RH, the scattering cross-section of an ammonium sulfate particle can be increased by a factor of five or more above that of the dry particle, due to large increases in size from uptake of water (Malm, 2001). Because of this, LWC is the most important contributor to direct radiative cooling by aerosols (Pilinis et al., 1995), currently thought to be $-0.45\,W\,m^{-2}$ ($-0.95\,W\,m^{-2}$ to $+0.05\,W\,m^{-2}$) (IPCC, 2013). LWC plays a large role in secondary aerosol formation for inorganic and possibly organic species by providing a large aqueous surface for increased gas uptake and a liquid phase where aqueous phase chemical reactions can result in products of lower vapor pressures than the absorbed gases. In the eastern US, the potential for organic gases to partition to LWC is greater than the potential to partition to particle-phase organic matter (Carlton and Turpin, 2013), and partitioning of water soluble organic carbon (WSOC) into the particle phase becomes stronger as RH (i.e., LWC) increases (Hennigan et al., 2008). Thus LWC enhances particle scattering effects directly by increasing particle cross sections and indirectly by promoting secondary aerosol formation (Nemesure et al., 1995).

The behavior of inorganic salts under variable RH is well established both experimentally and theoretically. It is known that dry inorganic salts (or mixtures thereof) exhibit a phase change, called deliquescence, when exposed to RH above a characteristic value. During deliquescence, the dry aerosol spontaneously transforms (at least partially) into an aqueous solution (Tang, 1976; Wexler and Seinfeld, 1991; Tang and Munkelwitz, 1993). In contrast, due to its chemical complexity that evolves with

ACPD
14, 27143–27193, 2014

atmospheric aging, the relationship of organics to LWC is not well characterized, and requires a parameterized approach. Despite the abundance and importance of LWC, it is not routinely measured. Thus, actual ambient particle total mass concentration is not well characterized. In general, LWC is measured by perturbing the in-situ RH. The loss of particle volume when RH is lowered is assumed to be solely due to evaporated water. Approaches for LWC measurements are classified into single particle size probes and bulk size quantification (Sorooshian et al., 2008). Single size particle probes provide more information, i.e., size resolved hygroscopic growth, and usually tend to be slow due to whole size range scanning. In contrast, bulk size measurements quantify the total water amount directly. The LWC measurement presented in this paper by nephelometers is a bulk measurement.

As part of the Southern Oxidant and Aerosol Study (SOAS), we made detailed measurements of particle organic and inorganic composition (Xu et al., 2014), aerosol hygroscopicity (Cerully et al., 2014), and indirect measurements of particle LWC. These data are used to first determine the particle water mass concentrations, which are then utilized in a thermodynamic model for predicting pH. This paper provides fine particle LWC and pH data, which are used in our other studies of secondary aerosol formation as part of SOAS (Cerully et al., 2014; Xu et al., 2014). In this analysis we use bulk properties and do not consider variability in parameters with particle size. Particle phase separations are also not considered, although they have been measured in bulk extracts of aerosols from the southeast (You et al., 2012). With ambient RHs typically higher than 60 %, formation of non-crystalline organic coatings over an aqueous core are possible, but glassy states are not expected. Good agreement between measured particle water and ammonia partitioning to predictions using the bulk properties (discussed below) suggests these assumptions are reasonable.

ACPD
14, 27143–27193, 2014

2 Data collection

2.1 Measurement sites

Aerosol measurements were conducted at the SEARCH Centerville site (CTR; 32.90289° N, 87.24968° W, altitude: 126 m), located in Brent, Alabama, as part of the SOAS (Southern Oxidant and Aerosol Study) study (http://soas2013.rutgers.edu). SOAS ground measurements were made from 1 June to 15 July in the summer of 2013. CTR is a rural site within a large forested region dominated by biogenic VOCs emission with minor local anthropogenic emissions and some transported plumes (sulfur, CO, biomass burning, mineral dust). It is representative of background conditions in southeastern US and chosen to investigate biogenic secondary organic aerosol (SOA) formation and its interaction with anthropogenic pollution from long range transport.

Additional measurements were also made at various sampling sites in and around the metropolitan Atlanta region from May 2012 to December 2012 as part of a large health study, Southeastern Center for Air Pollution and Epidemiology (SCAPE). A map of all the five sites is shown in Fig. 1. The measurement sites include:

1. A road-side (RS) site (33.775602° N, 84.390957° W), situated within 5 m from the interstate highway (I75/85) in midtown Atlanta and chosen to capture fresh traffic emissions.

2. A near-road site (GIT site, 33.779125° N, 84.395797° W), located on the rooftop of the Ford Environmental Science and Technology (EST) building at Georgia Institute of Technology (GIT), Atlanta, roughly 30 to 40 m a.g.l., 840 m from the RS site.

3. Jefferson Street (JST) (33.777501° N, 84.416667° W), a central SEARCH site representative of the Atlanta urban environment, located approximately 2000 m west of the GIT site.

ACPD
14, 27143–27193, 2014

4. Yorkville (YRK) (33.928528° N, 85.045483° W), the rural SEARCH pair of JST, situated in an agricultural region approximately 70 km west from the JST, GIT and RS sites.

More information on the SEARCH sites can be found in (Hansen et al., 2003, 2006). We first focus on the SOAS campaign data, where the widest range of instrumentation was deployed (http://soas2013.rutgers.edu), to develop a comprehensive method of predicting LWC and pH as well as assessing their uncertainties. The approach is then applied to the SCAPE site data to provide a broader spatial and temporal assessment of $PM_{2.5}$-particle water and pH in the southeastern US.

2.2 Instrumentation

PILS-IC. $PM_{2.5}$ or PM_1 (particles with aerodynamic diameters < 2.5 or 1.0 µm at ambient conditions) water soluble ions were measured by a Particle-Into-Liquid-Sampler coupled with an Ion Chromatograph (PILS-IC; Metrohm 761 Compact IC). Similar setups are described in previous field studies (Orsini et al., 2003; Liu et al., 2012). Metrosep A Supp-5, 150/4.0 anion column and C 4, 150/4.0 cation column (Metrohm USA, Riverside, FL) were used to separate the PILS liquid sample anions (sulfate, nitrate, chloride, oxalate, acetate, formate) and cations (ammonium, sodium, potassium, calcium, magnesium) at a 20 min duty cycle. The PILS sample air flow rate was 16.8 ± 0.4 L min^{-1}. URG (Chapel Hill, NC) cyclones were used to provide PM cut sizes of $PM_{2.5}$ for the 1st half of field study (1 to 22 June) and PM_1 for the latter half (23 June to 15 July). Honeycomb acid (phosphoric acid)- and base (sodium carbonate)-coated denuders removed interfering gases before entering the PILS. The sample inlet was ~ 7 m a.g.l. and ~ 4 m long. The sampling line was insulated inside the trailer (typical indoor T was 25 °C) and less than 1 m in length to minimize possible changes in aerosol composition prior to measurement. Periodic 1 h blank measurements were made every day by placing a HEPA filter (Pall corp.) on the cyclone inlet. All data were blank corrected. The PILS IC was only deployed for the SOAS study.

ACPD
14, 27143–27193, 2014

AMS. A High-Resolution Time-of-Flight Aerosol Mass Spectrometer (HR-ToF-AMS, Aerodyne Research Inc., hereafter referred to as "AMS") provided real time, quantitative measurements of the non-refractory components of submicron aerosols (DeCarlo et al., 2006; Canagaratna et al., 2007). In brief, particles were first dried (RH < 20 %) and then immediately sampled through an aerodynamic lens into the high vacuum region of the mass spectrometer, then transmitted into a detection chamber where particles impact on a hot surface (600 °C). Non-refractory species are flash vaporized and then ionized with 70 eV electron impact ionization. The generated ions are extracted into the time-of-flight mass spectrometer. Further details on the AMS setup and data processing can be found in Xu et al. (2014).

CCNc. The particle hygroscopic parameter, κ (Petters and Kreidenweis, 2007), used to infer the hygroscopic properties (liquid water associated with organics), was obtained from size-resolved CCN measurements obtained with a Droplet Measurement Technologies Continuous-Flow Streamwise Thermal Gradient Cloud Condensation Nuclei counter (CFSTGC, referred to hereafter as CCNc) (Roberts and Nenes, 2005; Lance et al., 2006). The CCNc exposes aerosols to a known supersaturation, then counts the activated particles that grow rapidly to droplet size. Theory can be used to parameterize the water phase properties (here, expressed by κ; Petters and Kreidenweis, 2007) of the organic aerosol, based on the size of particles that form CCN and their composition. The details of the CCNc setup and data analysis procedure can be found in Cerully et al. (2014).

Ambient vs. dry nephelometers. $PM_{2.5}$ aerosol light scattering coefficients (σ_{sp}) were measured online with two different nephelometers (Radiance Research M903) to infer LWC. Both were operated at nominally 3 L min^{-1} controlled by critical orifices and vacuum pumps located some distance away from the instruments. Particle dry scattering was measured with a nephelometer located in the air-conditioned sampling trailer operated with a nafion dryer upstream, which maintained an RH of 31.5 ± 1.9 % (study mean ± SD, n = 12 464 based on 5 min averages). The other was situated in a small white 3-sided wooden shelter located a distance away from all building to provide

ACPD
14, 27143–27193, 2014

a scattering measurement at ambient T and RH. Both nephelometers were calibrated by CO_2 prior to the SOAS field campaign. Typical uncertainty is 3 % for scattering coefficients (Mitchell et al., 2009). In addition, the nephelometer RH sensors were calibrated by placing the sensors in a closed container above aqueous saturated salt solutions that had reached equilibrium (measurements made in a thermally insulated container after a period of a few hours). Solution temperatures were monitored. Details on the calibration results are provided in Supplement. Recorded RH was corrected by the resulting calibration results.

2.3 Determining LWC from nephelometers

Particle water was inferred from the ratio of wet and dry $PM_{2.5}$ (URG cyclones) scattering coefficients (σ_{sp}) measured by the two nephelometers (defined here as aerosol hygroscopic growth factor, $f(\mathrm{RH}) = \sigma_{sp(wet)}/\sigma_{sp(dry)}$, where $\sigma_{sp(wet)}$ and $\sigma_{sp(dry)}$ are particle scattering coefficients in ambient and dry RH conditions respectively) following the method developed by other investigators (Carrico et al., 1998; Kotchenruther and Hobbs, 1998; Carrico et al., 2000; Malm, 2001; Sheridan, 2002; Magi, 2003; Kim et al., 2006). A difference between ambient and dry scattering coefficients is assumed to be caused solely by loss of water. Detailed derivations are provided in the Supplement. $f(\mathrm{RH})$ is related to the measured particle scattering efficiencies (Q) and average particle diameter ($\overline{D_p}$) by;

$$\overline{D_{p,wet}} = \overline{D_{p,dry}} \sqrt{f(\mathrm{RH}) Q_{wet}/Q_{dry}} \quad (1)$$

Q_{wet}, $\overline{D_{p,wet}}$ are scattering efficiency and average particle diameter under ambient conditions, while Q_{dry}, $\overline{D_{p,dry}}$ represent the dry condition. The method is based on the fact that for fine particles, scattering is most effective by particles in the accumulation mode and can be related to scattering efficiencies and the diameter of average surface, for both wet and dry particle size distributions. Assuming that Q_{wet} and Q_{dry} are of similar

ACPD
14, 27143–27193, 2014

magnitude, it follows then that;

$$\overline{D_{\mathrm{p,wet}}} = \overline{D_{\mathrm{p,dry}}}\sqrt{f(\mathrm{RH})} \quad (2)$$

Since the LWC is equal to the difference between wet and dry particle volume, we get;

$$\mathrm{LWC} = [f(\mathrm{RH})^{1.5} - 1]m/\rho_{\mathrm{p}} \quad (3)$$

where m and ρ_{p} are dry particle mass and density, respectively. For SOAS, dry $PM_{2.5}$ mass concentrations measured by a TEOM (Atmospheric Research & Analysis Inc.) were used. Particle density, ρ_{p}, was computed from the particle composition, including AMS total organics, ammonium, and sulfate, which accounted for 90 % of the measured $PM_{2.5}$ (TEOM) dry mass (SOAS study mean). A typical organic density 1.4 g cm^{-3} is assumed (Turpin and Lim, 2001; King et al., 2007; Engelhart et al., 2008; Kuwata et al., 2012; Cerully et al., 2014), and the density of ammonium sulfate is assumed to be 1.77 g cm^{-3} (Sloane et al., 1991; Stein et al., 1994). Particle density, ρ_{p}, was calculated to be 1.49 ± 0.04 g cm^{-3} (n = 4393) using mass fractions (ε):

$$\rho_{\mathrm{p}} = \frac{1}{\varepsilon(\mathrm{NH_4} + \mathrm{SO_4})/1.77 + \varepsilon(\mathrm{Organics})/1.4}(\mathrm{g\,cm^{-3}}) \quad (4)$$

The time-resolved composition data shows that dry particle density did not have a significant diurnal variability (± 2.7 %, SD/mean). (Note, SO_4 stands for sulfate in all its possible forms, from free to completely dissociated, the same applies to all other ions, e.g., NH_4, NO_3, etc.) In the following we refer to the particle water calculated by this method as f(RH)_water. The uncertainty of f(RH)_water is estimated to be 23 %, mainly caused by $Q_{\mathrm{wet}}/Q_{\mathrm{dry}}$ (~ 20 %), m (10 %), $\sigma_{\mathrm{sp(wet)}}/\sigma_{\mathrm{sp(dry)}}$ (4.2 %) (uncertainty for a single σ_{sp} measurement is 3 %, Mitchell et al., 2009), and ρ_{p} (2.7 %).

ACPD
14, 27143–27193, 2014

3 LWC prediction from aerosol composition

In most studies, such as SCAPE, particle water was not measured and must be determined based on aerosol composition. Both inorganic and organic components contribute to uptake of water vapor, establishing equilibrium for the ambient RH and T conditions. Thus, LWC is controlled by meteorological conditions and also by aerosol concentration and composition. Thermodynamic models, such as ISORROPIA-II, have been extensively used to predict LWC due to inorganic aerosol components (Fountoukis and Nenes, 2007). Contributions to LWC by organic components are typically based on an aerosol hygroscopicity parameter, κ, which is determined by CCN data. Here we refer to particle water associated with inorganics and organics as W_i and W_o, respectively. Total particle water ($W_i + W_o$) is taken as the sum of water associated with individual aerosol chemical components (sum of ions and lumped organics), with the assumption that the particles are internally mixed.

3.1 LWC from inorganic species

W_i was predicted by ISORROPIA-II (Nenes et al., 1998; Fountoukis and Nenes, 2007). ISORROPIA-II calculates the composition and phase state of an NH_4-SO_4-NO_3-Cl-Na-Ca-K-Mg-water inorganic aerosol in thermodynamic equilibrium with gas phase precursors. Chemical and meteorological data are necessary inputs. For our analysis at CTR, the inputs to ISORROPIA-II are the inorganic ions measured by the IC or AMS, RH measured by the outside Nephelometer, and temperature from the SEARCH site (ARA) meteorological data.

3.2 LWC from organic fraction

To determine the contributions to particle water by W_o, in SOAS the organic hygroscopicity parameter (κ_{org}) was measured based on the observed CCN activities of the organic fraction (Cerully et al., 2014) and in the following analysis diurnal three-hour

ACPD
14, 27143–27193, 2014

running averages are used in the calculation. (Diurnal plot is included in the Supplement as Fig. 5) W_o is calculated using the following equation (Petters and Kreidenweis, 2007).

$$W_o = \frac{m_s}{\rho_s} \frac{\kappa_{org}}{\left(\frac{1}{RH-1}\right)} \quad (5)$$

where m_s is the organic mass concentration from AMS (Xu et al., 2014), and a typical organic density (ρ_s) of 1.4 g cm^{-3} (Turpin and Lim, 2001; King et al., 2007; Engelhart et al., 2008; Kuwata et al., 2012; Cerully et al., 2014).

3.3 pH prediction

The thermodynamic model, ISORROPIA-II (Fountoukis and Nenes, 2007), is used to predict particle pH, based on calculated equilibrium particle hydronium ion concentration in the aerosol. To correct for the LWC associated with the organic aerosol (not considered in ISORROPIA-II), we recalculate pH by considering the predicted particle hydronium ion concentration per volume air (H^+_{air}) and total predicted water (W_i and W_o). The modeled concentrations are μg m^{-3} air for H^+_{air} and LWC. The pH is then,

$$pH = -\log_{10} H^+_{aq} = -\log_{10} \frac{1000 H^+_{air}}{W_i + W_o} \quad (6)$$

where H^+_{aq} (mol L^{-1}) is hydronium concentration in a aqueous solution. ISORROPIA-II has been tested in previous field campaigns where a suite of both gas and particle components were measured (Nowak et al., 2006; Fountoukis et al., 2009). The model was able to predict the equilibrium partitioning of ammonia (Nowak et al., 2006) in Atlanta and nitric acid (Fountoukis et al., 2009) in Mexico City within measurement uncertainty. For instance, $NH_{3(g)}$, $NH_{4(p)r}$, $HNO_{3(g)}$, and $NO_{3(p)}$ were within 10, 20, 80, and 20 % of measurements (Fountoukis et al., 2009). In this study, ISORROPIA-II was run in the

ACPD
14, 27143–27193, 2014

"Forward mode" for metastable aerosol. Forward mode calculates the equilibrium partitioning given the total concentration of species (gas + particle) together with RH and T as input. Reverse mode involves predicting the thermodynamic composition based only on the aerosol composition. Here, we use the Forward mode with just aerosol phase data input because it is less sensitive to measurement error than the Reverse mode (Hennigan et al., 2014). The W_i prediction stays the same (Reverse vs. Forward: slope = 0.993, intercept = −0.005, and R^2 = 0.99) no matter which approach is used. Gas phase input does have an important impact on the H^+_{air} calculation. ISORROPIA-II was tested with ammonia partitioning. Discussed in more detail below, here it is noted that we found that further constraining ISORROPIA-II with measured $NH_{3(g)}$ (You et al., 2014) resulted in a pH increase of 0.8 at CTR and that the predicted $NH_{3(g)}$ matched the measured $NH_{3(g)}$ well (slope = 1.07, intercept = −0.12, R^2 = 0.76). This also confirms that ISORROPIA-II predicts the pH in the ambient aerosol with good accuracy, as inputting the total (gas + aerosol) ammonium results in predictions that agree with those observed. This is also in agreement with findings of Hennigan et al. (2014) and Fountoukis et al. (2009), whom found that ISORROPIA-II reproduced the partitioning of ammonia and inorganic nitrate in Mexico City during the MILARGO campaign.

4 Results

4.1 Summary of meteorology and PM composition

Of the sites in the southeastern US discussed in this paper, CTR was the least influenced by anthropogenic emissions having the lowest black carbon (BC) concentrations (measured by a MAAP, Thermo Scientific, model 5012). At CTR, the mean BC = 0.26 ± 0.21 μg m^{-3} (± SD), whereas mean BC concentrations at the other rural site (YRK) was 0.36 μg m^{-3}. The representative Atlanta site (JST) BC was on average 0.71 μg m^{-3}, and higher for sites closer to roadways, 0.96 μg m^{-3} (GIT) and 1.96 μg m^{-3} (RS).

ACPD
14, 27143–27193, 2014

For the SOAS study period, mean T and RH were $24.7 \pm 3.3\,^{\circ}C$, $73.8 \pm 16.1\,\%$ (mean $\pm$ SD), respectively. This resulted in f(RH)_water level of $4.52 \pm 3.75\,\mu g\,m^{-3}$, with a maximum value of $28.41\,\mu g\,m^{-3}$. In comparison, SOAS mean dry $PM_{2.5}$ mass was $7.72 \pm 4.61\,\mu g\,m^{-3}$, implying that the fine aerosols were composed of roughly 37 % water on average. Mean T and RH for SCAPE sites are listed in Table 3. Summer T means were all above $21\,^{\circ}C$, including CTR. RH means were all high (> 60 %) for summer and winter, which is typical for the southeastern US.

A more comprehensive suite of ions will provide a better prediction of W_i. However, in the southeastern US, inorganic ions are currently dominated by sulfate and ammonium. During SOAS, the PILS-IC provided a more comprehensive and accurate measurement of water-soluble ions than AMS, which measured only non-refractory sulfate, ammonium, nitrate, and chloride. Refractory, but water soluble ions, such as sodium and associated chloride, and crustal elements including calcium, potassium, and magnesium were present in PM_1, but in very low concentrations. Contributions of these ions are more important in $PM_{2.5}$ than for PM_1, which tend to reduce aerosol acidity. For instance, Na has a significantly higher mean in $PM_{2.5}$ at $0.056\,\mu g\,m^{-3}$ (1st half of SOAS study) than $0.001\,\mu g\,m^{-3}$ in PM_1 (2nd half of SOAS study) at CTR. Four, one day-long, dust events (12, 13, 16, and 21 June) in the SOAS data set have been excluded from this analysis as assumptions relating to internal mixing of $PM_{2.5}$ components are less valid in these cases. Excluding these days, mean Na $PM_{2.5}$ drops to $0.024\,\mu g\,m^{-3}$.

If the fraction of the refractory ions (e.g., Na, Ca, K, Mg) is negligible compared to the SO_4, NH_4, and NO_3, the AMS data sufficiently constrains particle composition for thermodynamic calculations; this apparently is the case for most of the time in the southeast (Supplement Sect. 5). For PM_1 SO_4 and NH_4, AMS and PILS-IC were in good agreement (sulfate slopes within 20 %, $R^2 = 0.90$; ammonium within 1 %, $R^2 = 0.81$). Similar agreement was also found for AMS PM_1 SO_4 and NH_4 vs. PILS-IC $PM_{2.5}$ SO_4 and NH_4. (See Fig. 2 for comparison of complete data set.) These data indicate little SO_4 and NH_4 between the 1.0 and 2.5 µm size range ($PM_{2.5}$–PM_1). Because of the agreement between these dominant ions, ISORROPIA-II-predicted W_i for all ions

ACPD
14, 27143–27193, 2014

measured with the PILS-IC throughout the study (includes both PM_1 and $PM_{2.5}$) agreed with W_i based on AMS inorganic species (i.e., only ammonium and sulfate) having an orthogonal slope of 1.18, Fig. 2c.

4.2 LWC uncertainty

In estimating the water uncertainty, we consider W_i and W_o separately. The uncertainty of W_i is estimated by propagating the measurement uncertainty of ions and RH through the ISORROPIA-II thermodynamic model by finite perturbations about the model base state. Uncertainties of ions were estimated by difference between IC-ions and AMS-ions, as well as PILS-IC measurement uncertainty (Table 2). Na is excluded because it is not measured by the AMS. PILS-IC instrumental uncertainty is estimated to be 15 % from the variability in standards (variability is calibration slopes), blanks, sample airflow rate, and liquid flow rate (one SD). The total ion uncertainties are listed in Table 2. SO_4 has a higher uncertainty, at 25 %, than the rest, which are at 15 %. These combined uncertainties lead to an W_i uncertainty of 25 % (Fig. 3), which is the same as the SO_4 uncertainty, since as the most hygroscopic ion it controls W_i uptake. Although the AMS data set does not include Na and crustal elements, it is still generally capable of predicting W_i as it measures the most hygroscopic and abundant ions SO_4, NH_4, and NO_3 (Fig. 2).

For the SOAS study, the RH probe in the ambient nephelometer (Humitter 50U, VAISALA Inc.) has a stated max uncertainty of 5 % at RH = 90 %. RH biases with respect to environment conditions can also occur due to placement of the probe. Based on RH comparisons between ARA, Rutgers (Nguyen et al., 2014), and the Georgia Tech instrumentation, a systematic bias as large as 10 % is found. Given this, we consider an RH probe factory uncertainty (5 %) as a typical value and inter-comparison difference (10 %) as an extreme condition. In this analysis, RH was adjusted by ±5 and ±10 % and W_i recalculated (Fig. 4). A ±5 % perturbation in RH leads to a 91 % (slope – 1, see Fig. 7) error for 5 % perturbation above the measured value (1.05 RH) and 29 % error for a perturbation below the measured value (0.95 RH). We take 60 % as aver-

ACPD
14, 27143–27193, 2014

age uncertainty. Higher uncertainty is introduced with increasing RH, owning to the exponential growth of LWC with RH and results in the asymmetric LWC uncertainty. Combining W_i uncertainty from ions (25 %) and RH (60 %), the overall uncertainty is calculated as 65 %.

The uncertainty sources for W_o are κ, ρ_s, m_s, and RH (Eq. 5). The uncertainties of these parameters are estimated to be 20 % (Cerully et al., 2014), 10, 20, and 5 % (from above), respectively. In summary, the overall uncertainty of W_o is 30 %.

The total uncertainty of LWC can be expressed as a sum of W_i and W_o uncertainties, where ε_i is the mass fraction. ε_{W_o} was found to be 36 % and ε_{W_i} was 64 %.

$$\frac{\delta_{\mathrm{LWC}}}{\mathrm{LWC}} = \sqrt{\left(\varepsilon_{W_i}\frac{\delta_{W_i}}{W_i}\right)^2 + \left(\varepsilon_{W_o}\frac{\delta_{W_o}}{W_o}\right)^2} \quad (7)$$

Given the above, $\frac{\delta_{\mathrm{LWC}}}{\mathrm{LWC}}$ is 43 %. This method of assessing predicted LWC uncertainty can be applied to SCAPE sites as well. The specific predicted LWC at SCAPE sites were calculated and are listed in Table 3. W_i uncertainty associated with ions is the same as noted above, 25 %, because it is estimated by PILS-IC and AMS differences. Similar uncertainties in W_i at the SCAPE sites are expected if RH uncertainties are similar at all sites.

4.3 pH uncertainty

As pH is based on H^+_{air} and LWC, the uncertainty of pH can be estimated from these two parameters. We applied the adjoint model of ISORROPIA, ANISORROPIA (Capps et al., 2012), to quantify the sensitivity of predicted H^+ to the input aerosol species at the conditions of the thermodynamic calculations. pH uncertainty resulted from aerosol composition is then determined by propagating the input parameter uncertainties, using ANISORROPIA sensitivities, to the corresponding H^+ and pH uncertainty.

We now assess how pH of $PM_{2.5}$ is affected by using an incomplete measurement of ionic species by comparing the pH predicted based on the more complete suite of ions

ACPD
14, 27143–27193, 2014

measured by the PILS-IC vs. the AMS, during SOAS. Sensitivities of aerosol species to H^+ were calculated by ANISORROPIA with PILS-IC data and presented as partial derivatives (Table 2). Higher sensitivity values imply the inorganic ion is more important for ion balance. In the SOAS study, H^+ is most sensitive to SO_4, and then NH_4, as they were the major ions. Uncertainties of ions were estimated by the difference between IC-ions and AMS-ions, as well as PILS-IC measurement uncertainty. Since Na is not measured by AMS, we cannot estimate the difference between PILS-IC and AMS. The loadings and sensitivities of NO_3 and Cl were very low, so they are assumed not to contribute much to $\frac{\delta_{H^+}}{H^+}$. Given this, $\frac{\delta_{H^+}}{H^+}$ is determined by;

$$\frac{\delta_{H^+}}{H^+} = \sqrt[2]{\left(\frac{\partial H^+}{\partial SO_4}\frac{\delta_{SO_4}}{SO_4}\right)^2 + \left(\frac{\partial H^+}{\partial NH_4}\frac{\delta_{NH_4}}{NH_4}\right)^2 + \left(\frac{\partial H^+}{\partial Na}\frac{\delta_{Na}}{Na}\right)^2} \quad (8)$$

Based on the input for Eq. (8) (Table 2), $\frac{\delta_{H^+}}{H^+}$ is estimated as 14 %. LWC is most sensitive to RH fluctuations, so it is considered the main driver of LWC uncertainty in the pH calculation. As discussed, we artificially adjusted RH by ±5 and ±10 % (10 % is considered an extreme condition). H^+, W_i, W_o, as well as pH were all recalculated using 90, 95, 105, and 110 % of the actual measured RH. RH + 5 % and RH – 5 % lead to 12 and 6 % variation in pH based on orthogonal regression slopes, respectively (Fig. 5). RH – 10 % results in only 10 % variation, however, RH + 10 % results in a 45 % variation, and the coefficient of determination (R^2) between pH calculated based on RH + 10 % and original RH drops to only 0.78, while for all other cases $R^2 > 0.96$. The disproportionately large effect of the positive uncertainty is caused by the exponential increase of LWC with RH, as RH reaches high levels (> 90 %). Assuming the stated manufacturer uncertainty (5 %) for our RH uncertainty, pH uncertainty is estimated to be 6–12 %. We take 12 % as $\frac{\partial pH}{\partial LWC}\delta_{LWC}$ for further calculations.

SO_4 was found to contribute the most to $\frac{\delta_{H^+}}{H^+}$. NH_4 and Na followed. SO_4 and NH_4 are the two most abundant inorganic components in aerosols and controlling aerosol

ACPD
14, 27143–27193, 2014

acidity. Finally, the total pH uncertainty is the combination of LWC and the uncertainty associated with H^+, which is computed from the definition of pH (Eq. 6).

$$\frac{\delta_{pH}}{pH} = \sqrt[2]{\left(\frac{\partial pH}{\partial H^+}\delta_{H^+}\right)^2 + \left(\frac{\partial pH}{\partial LWC}\delta_{LWC}\right)^2} \quad (9)$$

where $\frac{\partial pH}{\partial H^+}$ can be derived from Eq. (6) as

$$\frac{\partial pH}{\partial H^+} = -\frac{1}{2.303}\frac{1}{\frac{H^+}{LWC}}\frac{1}{LWC} = -\frac{1}{2.303}\frac{1}{H^+} \quad (10)$$

From Eq. (9) and the uncertainties of H^+ and LWC (Eqs. 7 and 8), we estimate the pH uncertainty for the SOAS dataset to be 13 % (based on the specific uncertainties considering here). pH uncertainties at SCAPE sites were also assessed via this method. As discussed above, $\frac{\delta_{H^+}}{H^+}$ was found to be 14 % for the SOAS study, due to IC and AMS data set differences and PILS-IC instrumental uncertainty. This same uncertainty is applied to SCAPE, where no PILS-IC data were available. Because aerosol compositions at all sites are similar, based on filter IC analysis (Fig. S6), similar sensitivities of H^+ to ions are expected. However, actual uncertainty for each sampling period is possibly higher due to higher loadings of refractory ions at SCAPE sites due to contributions from urban emissions. Refractory ions not measured by the AMS (i.e. Na, K, Ca, Mg), having a minor effect on predicting LWC, but may have an important effect on pH in locations (e.g. pH higher) where they could substantially contribute to the overall ion balance.

pH uncertainty in different seasons. Recall at CTR, 10 % RH uncertainty can result in a pH prediction error of up to 45 % due to the high RHs observed during the study. We estimated pH uncertainty from W_i and W_o by +10 % RH for each SCAPE site. As Table 3 shows, the pH uncertainty associated with RH is much lower in winter (only 1–3 %) than summer (20–40 %), although RH averages were similar, e.g. JST in May (67 ± 19 %)

ACPD
14, 27143–27193, 2014

and Nov (63 ± 19 %), with even higher RH in winter at YRK. Total pH uncertainty at all SCAPE sites are calculated by the same method as CTR. Table 3 shows that higher RH and T result in larger pH uncertainty. In summer, pH uncertainty is mainly caused by RH; while in winter, it can be attributed mostly to uncertainty in ion concentrations. pH predicted for the SCAPE sites likely has a systematic bias of roughly −1 because $NH_{3(g)}$ is not included in the ISORROPIA-II calculation (recall including $NH_{3(g)}$ increased the CTR pH by 0.8). At JST, YRK, GIT, and RS sites, summer mean pH were between 0 and 0.3. Adding 1 pH unit of systematic bias makes pH at these southeastern sites between 1 and 1.3, which is consistent with the CTR pH of 0.94 ± 0.59 (± SD). $NH_{3(g)}$ does not significantly affect the LWC prediction (W_i predicted without $NH_{3(g)}$ vs. W_i predicted with $NH_{3(g)}$: slope = 1.00, intercept = −0.01 μg m^{-3}, R^2 = 0.98).

4.4 LWC comparison to predictions and seasonal and diurnal trends in the southeast

Several LWC measurements were made at CTR during SOAS. In addition to f(RH)_water (4.52 ± 3.75 μg m^{-3}), particle water was quantified with a Semi-volatile Differential Mobility Analyzer (SVDMA). With this method, a SOAS study mean particle water concentration of 4.27 ± 3.69 μg m^{-3} (± SD) was obtained (Nguyen et al., 2014). The orthogonal regression between these two measurements (SVDMA water vs. f(RH)_water) has slope = 0.91, intercept = −0.03, r = 0.59. Differences could be caused by differences in size-resolved composition (particle composition beyond PM_1 that contributes LWC; SVDMA scans up to 1.1 μm, while f(RH)_water is based on $PM_{2.5}$), instrument sample heating (i.e., the degree to which the instrument was close to ambient conditions, especially when ambient RH was high, hence most sensitive to slight T differences), and differences in RH probe calibrations.

The particle water predicted from the sum of W_i and W_o agreed well with f(RH)_water. That is, the total predicted water was highly correlated and on average

ACPD
14, 27143–27193, 2014

within 10 % of the measured water, with slope = 0.91, intercept = 0.46, $r = 0.87$ (see Fig. 6).

Since excluding refractory ions (Sect. 4.1) and not considering gas phase species in the ISORROPIA-II calculations do not significantly affect the LWC prediction, its comparison across sites is less uncertain than pH. CTR total LWC is predicted to be $5.09 \pm 3.76\,\mu g\,m^{-3}$. LWC predictions at all the other sites are shown in Table 3, providing insights on seasonal trends of LWC in the southeast. The overall summer LWC mean was $5.02\,\mu g\,m^{-3}$ and winter mean $2.22\,\mu g\,m^{-3}$.

The diurnal variation of LWC contributed by W_i and W_o, along with total measured water, ambient T, RH, and solar radiation at CTR is shown in Fig. 7. Predicted and measured LWC trends are in good overall agreement, although the largest discrepancy was observed during the daytime when LWC level was low and more difficult to measure and accurately predict. Nighttime RH median values were between 85 and 90 % and resulted in significant water uptake that reached a peak just after sunrise near 7.30 a.m. (LT). The dramatic peak in LWC starting at roughly 5 a.m., reaching a maximum between 7.30 and 8 a.m. is likely due to RH increasing above 90 %, at which point uptake of water rapidly increases with increasing RH. The similar rapid hygroscopic growths before sunrise were also observed at GIT, RS, and JST (November). After sunrise, rising temperatures lead to a rapid drop in RH, resulting in rapid loss of particle water. LWC reached lowest levels in the afternoon $\sim 2\,\mu g\,m^{-3}$, only 20 % of the peak value. W_o varied more than W_i; W_o diurnal variation ratio (max / min) was 13.1 compared to 4.1 for W_i.

W_o was significant, accounting for on average 29–39 % of the total $PM_{2.5}$ particle water for all our sites (Fig. 8 and Table 3). Note that, W_o at SCAPE sites were calculated by in-situ AMS measurement at each SCAPE site and measured κ_{org} mean (0.126) at CTR, due to lack of CCNc. Figure 8 shows that W_o is related to the organic mass fraction. W_o is comparable to W_i at night. In contrast, it was only 33 % of W_i during the daytime (Fig. 7). The significant fraction, even during daytime, indicates organic aerosol components will have a considerable contribution to aerosol radiative forcing.

ACPD
14, 27143–27193, 2014

Although organics are less hygroscopic than ammonium sulfate, a large fraction of the $PM_{2.5}$ (~ 70 %) was organic, making W_o contributions important. Of the organic factors associated with W_o, Cerully et al. (2014) showed that MO-OOA (more-oxidized oxygenated organic aerosol, also referred to as LVOOA, low-volatile oxygenated organic aerosol) and Isoprene-OA (isoprene derived organic aerosol) were twice as hygroscopic as LO-OOA (less-oxidized oxygenated organic aerosol, also referred to as SVOOA, semi-volatile oxygenated organic aerosol). The LWC associated with MO-OOA and Isoprene-OA account for ~ 60 and ~ 30 % of total W_o in the daytime, respectively.

4.5 Ammonia partitioning, model validation and pH bias when gas/particle data not included

As noted earlier, ISORROPIA-II calculations at CTR for the SOAS study were evaluated by comparing measured and predicted $NH_{3(g)}$. Although NH_4 and $NH_{3(g)}$, along with other aerosol components, are input into the model, comparing ambient NH_4 and $NH_{3(g)}$ to model predictions is not a circular analyses. For each observed data point, the model calculates total ammonia from the NH_4 and $NH_{3(g)}$ input, and then calculates the gas-particle ammonia partitioning assuming equilibrium and the other various assumptions/limitations associated with the model. Figure 9 shows the SOAS study time series of measured and predicted $NH_{3(g)}$ and the fraction of ammonia in the gas phase ($NH_{3(g)}/(NH_{3(g)} + NH_{4(p)})$). Diurnal changes in the gas fraction can be seen and are likely due to diurnal changes in particle pH, discussed below. Periods when almost all ammonia was in the gas phase (ratio near 1) are related to precipitation events (10, 24, 28 June and 3, 4 July) when aerosol concentrations were very low. Not including these events, the study mean (± SD) fraction ammonia in the gas phase was 0.41 (±0.16) (median value is also 0.41). These results provide confidence in ISORROPIA-II calculations of particle pH, and demonstrate the utility of including both measurements of particle and gas phases in these types of studies.

ACPD
14, 27143–27193, 2014

When gas and particle data are not available, pH predictions are likely not as accurate (Hennigan et al., 2014). Running ISORROPIA-II in the forward mode, but with only aerosol concentrations as input, may result in a bias in predicted pH due to repartitioning of ammonia in the model. In the southeast, where pH is largely driven by SO_4 and NH_4, the aerosol NH_4 input will be partitioned in the model between gas and particle phases to establish equilibrium. Sulfate repartitioning does not occur since it is non-volatile. Thus NH_4 will be lost from the particle and a lower pH predicted. At CTR ammonia partitioning has been included in all model runs, but as no $NH_{3(g)}$ was available for SCAPE, the pH is likely biased at these sites by roughly −1. In the following, all pHs reported for SCAPE are corrected for this bias (i.e., pH increased by 1). Note that ammonia partitioning does not significantly affect the LWC prediction (W_i predicted without $NH_{3(g)}$ vs. W_i predicted with $NH_{3(g)}$: slope = 1.00, intercept = $-0.01\ \mu g\,m^{-3}$, $R^2 = 0.98$).

4.6 pH diurnal, seasonal, and spatial trends in the southeast

At CTR, the aerosol was highly acidic, with predicted mean pH = 0.94 ± 0.59 (± SD). The minimum and maximum pH were −0.94 and 2.23 respectively, and pH varied by approximately 1 on average throughout the day (Fig. 10). That is, the H^+_{air}/LWC ratio increased by a factor of 10 from night to day. LWC max / min ratio was 5, whereas H^+ diurnal variation was significantly less (Fig. 10), indicating that the diurnal pattern in pH was driven mainly by particle water dilution. This is further demonstrated in Fig. 11, which shows the diurnal variation in the NH_4/SO_4 molar ratio (the main ions driving pH), with only slightly lower ratios during the day. The study mean (± SD) NH_4/SO_4 molar ratio was 1.4 (±0.5). As LWC is mainly controlled by RH and temperature, the pH diurnal variation was thus largely driven by meteorological conditions, not aerosol composition. Because of this, a simple ion balance or per volume air concentration of aerosol hydronium ion (H^+_{air}) alone cannot be used as a proxy for pH in the particle.

At the SCAPE sites, JST, YRK, GIT, and RS, summer mean pHs were between 1 and 1.3, similar to CTR (mean of 0.94). In winter the pHs (mean between 1.8 and 2.2) were higher by ∼ 1 unit. Although LWC was higher in summer, which tends to dilute H^+

ACPD
14, 27143–27193, 2014

and increase pH, summer pH was lower due to higher ion (i.e., sulfate) concentrations (Table 3). Similar diurnal pH patterns were seen at all sites in all seasons and follow the diurnal variations of particle water (Fig. 12). Overall the pH in the southeast is very low, between 1 and 2 (mean), in both rural and urban environments. pH values in summer at various sites were similar (1 to 1.3), suggesting a fairly homogeneous distribution of acidity due to spatially uniform sulfate in the southeastern US (Zhang et al., 2012). In winter the diurnal range in pH was roughly 2, while the diurnal range in summer was smaller, with pH varying by roughly 1.

These acidic aerosols in the southeast will affect a variety of processes. For example, aerosol acidity strongly shifts the partitioning of $HNO_{3(g)}$ to the gas phase resulting in low nitrate aerosol levels in the southeast during summer (the higher summertime temperature also plays a secondary role). Aerosol acidity also impacts the gas-particle partitioning of semi-volatile organic acids. (Note, organic acids are not considered in our model, under these acidic conditions (pH = 1) their contributions to the ion balance (hence pH) are expected to be negligible. Because the pK_a($pK_a = -\log_{10} K_a$, K_a referred as acid dissociation constant) of trace organic acids are > 2 (e.g. pK_a of formic acid, one of the strongest organic acids, is 3.75, Bacarella et al., 1955), low pH prevents dissociation of the organic acids. Since H^+ is involved in aqueous phase reactions, low pH can affect reaction rates by providing more protons. Investigators have found that isoprene-OA formation is acid-catalyzed and sulfuric acid participates in the reaction as a proton donor in chamber studies (Surratt et al., 2007). However, aerosol acidity may not be the limiting factor of isoprene-OA formation in the southeastern US, owning to the consistently very low pH (Karambelas et al., 2014; Xu et al., 2014). Finally, low pH can affect the solubility of trace metals found in the insoluble fraction of aerosol (e.g., mineral dust) such as Fe and Cu, which possibly increases the toxicity of the redox metals (Ghio et al., 2012; Verma et al., 2014) and may have a long term effect on nutrient distributions (Meskhidze et al., 2003, 2005; Nenes et al., 2011; Ito and Xu, 2014).

ACPD
14, 27143–27193, 2014

Finally, the effect of aerosol sources of particle water on pH can also be delineated. pH calculated just by W_i alone will be affected by an underestimation of particle water, resulting in a slightly lower pH (Fig. 13). W_o is on average 29 to 39 % of total water at all sites, as a result pH increases by 0.15 to 0.23 units when W_o is included. pH based on W_i is highly correlated with pH for total water ($W_i + W_o$) ($R^2 = 0.97$, Fig. 14). This indicates that if organic mass and κ_{org} are not available, ISORROPIA-II run with only ion data will give a reasonable estimate of pH, since both H^+_{air} and W_i are outputs of ISORROPIA-II, while W_o is predicted based on organic mass and κ_{org}. Accurate temperature and RH are still necessary inputs, especially when RH is high.

5 Conclusions

Because particle pH is important and difficult to measure directly, by combining several models we present a comprehensive prediction method to calculate pH and include an uncertainty analysis. ISORROPIA-II is applied to calculate the concentration of H^+ and W_i from inorganic aerosol measurement, and CCN activity is used to predict W_o. The adjoint model of ISORROPIA, ANISORROPIA, is applied to determine sensitivities, which are used for propagating the measurement uncertainties to pH.

W_o accounted for a significant fraction of total LWC, at a mean of 35 % (±3 % SD) for SOAS and SCAPE field studies, indicating the importance of organic hygroscopic properties to aerosol scattering and direct radiative forcing. Although organics are less hygroscopic than sulfate and ammonium, the larger mass fraction of organics than inorganics promotes W_o uptake. Predicted LWC was compared to LWC determined from ambient vs. dry light scattering coefficients and a TEOM measuring dry $PM_{2.5}$ mass. In SOAS, measured LWC was highly correlated and in close agreement with the sum of W_i and W_o (slope = 0.91, $r = 0.87$). LWC showed a clear diurnal pattern, with a continuous increase at night (median nighttime LWC of 10 $\mu g\, m^{-3}$) reaching a distinct peak when RH reached a maximum near 90 % just after sunrise at the lowest ambient

ACPD
14, 27143–27193, 2014

temperature, followed by a rapid decrease and lower values during the day (median of $2\,\mu g\,m^{-3}$).

In the southeastern US, pH normally varies from 0.5 to 2 in the summer and 1 to 3 in the winter, indicating that the aerosol is acidic throughout the year. The minimum and maximum pH were −0.94 and 2.2 at CTR, respectively and varied from 1.5 at night to 0.6 on average in the day, mostly attributable to diurnal variation in RH and temperature. Mean ammonium to sulfate molar ratios were 1.4 ± 0.5 (SD) and roughly half the ammonia was in the gas phase ($NH_{3(g)}/(NH_{3(g)} + NH_{4(p)}) = 41 \pm 16\,\%$, mean ± SD). pH throughout the southeast (CTR excluded) was estimated based on a limited data set at an estimated uncertainty of 9–49 % and a systematic bias of −1 if $NH_{3(g)}$ is not included in the thermodynamic model run in forward mode. pH can still be predicted with only aerosol measurements, but a 1-unit pH increase adjustment is recommended for the southeastern US. pH has a diurnal trend that follows LWC, higher (less acidic) at night and lower (more acidic) during the day. pH was also generally higher in the winter (∼ 2) than summer (∼ 1). These low pHs have significant implications on gas-aerosol partitioning, acid-catalyzed reactions including isoprene-OA formation, and trace metal mobilization.

The Supplement related to this article is available online at doi:10.5194/acpd-14-27143-2014-supplement.

Acknowledgements. This work was supported by the NSF under grant number 1 242 258 as part of the SOAS campaign. GIT SOAS Researchers were also supported by a US EPA STAR grant R835410 and NOAA CPO Award NA10OAR4310102. Measurements at other sites in the southeast were part of the EPA-supported SCAPE Clean Air Center, made possible through US EPA grant R834799. The content of this publication are solely the responsibility of the grantee and do not necessarily represent the official views of the US EPA. Further, US EPA does not endorse the purchase of any commercial products or services mentioned in the publication. SLC was supported by an appointment to the Research Participation Program at the Office

ACPD
14, 27143–27193, 2014

of Research and Development, US EPA, administered by ORISE. SHL acknowledges funding support from NSF (AGS-1 241 498). AB acknowledges support within the framework of the Action "Supporting Postdoctoral Researchers" of the Operational Program "Education and Lifelong Learning" (Action's Beneficiary: General Secretariat for Research and Technology), and is co-financed by the European Social Fund (ESF) and the Greek State. We wish to thank the Southeastern Aerosol Research and Characterization (SEARCH) personnel for their many contributions supporting the field deployments.

References

Bacarella, A. L., Grunwald, E., Marshall, H. P., and Purlee, E. L.: The potentiometric measurement of acid dissociation constants and pH in the system methanol-water, pK_a values for carboxylic acids and anilinium ions, J. Org. Chem., 20, 747–762, doi:10.1021/Jo01124a007, 1955.

Canagaratna, M. R., Jayne, J. T., Jimenez, J. L., Allan, J. D., Alfarra, M. R., Zhang, Q., Onasch, T. B., Drewnick, F., Coe, H., Middlebrook, A., Delia, A., Williams, L. R., Trimborn, A. M., Northway, M. J., DeCarlo, P. F., Kolb, C. E., Davidovits, P., and Worsnop, D. R.: Chemical and microphysical characterization of ambient aerosols with the aerodyne aerosol mass spectrometer, Mass Spectrom. Rev., 26, 185–222, doi:10.1002/mas.20115, 2007.

Capps, S. L., Henze, D. K., Hakami, A., Russell, A. G., and Nenes, A.: ANISORROPIA: the adjoint of the aerosol thermodynamic model ISORROPIA, Atmos. Chem. Phys., 12, 527–543, doi:10.5194/acp-12-527-2012, 2012.

Carlton, A. G. and Turpin, B. J.: Particle partitioning potential of organic compounds is highest in the Eastern US and driven by anthropogenic water, Atmos. Chem. Phys., 13, 10203–10214, doi:10.5194/acp-13-10203-2013, 2013.

Carrico, C. M., Rood, M. J., and Ogren, J. A.: Aerosol light scattering properties at Cape Grim, Tasmania, during the First Aerosol Characterization Experiment (ACE 1), J. Geophys. Res., 103, 16565, doi:10.1029/98jd00685, 1998.

Carrico, C. M., Rood, M. J., Ogren, J. A., Neususs, C., Wiedensohler, A., and Heintzenberg, J.: Aerosol optical properties at Sagres, Portugal during ACE-2, Tellus B, 52, 694–715, doi:10.1034/j.1600-0889.2000.00049.x, 2000.

ACPD
14, 27143–27193, 2014

Cerully, K. M., Bougiatioti, A., Hite, J. R., Guo, H., Xu, L., Ng, N. L., Weber, R. J., and Nenes, A.: On the link between hygroscopicity, volatility, and oxidation state of ambient and water-soluble aerosol in the southeastern United States, submitted to Atmos. Chem. Phys. Discuss., 2014.

Clegg, S. L., Brimblecombe, P., and Wexler, A. S.: Thermodynamic model of the system H^+-NH_4^+-SO_4^{2-}-NO_3^--H_2O at tropospheric temperatures, J. Phys. Chem. A, 102, 2137–2154, doi:10.1021/Jp973042r, 1998.

Czoschke, N. M. and Jang, M.: Acidity effects on the formation of α-pinene ozone SOA in the presence of inorganic seed, Atmos. Environ., 40, 4370–4380, doi:10.1016/j.atmosenv.2006.03.030, 2006.

DeCarlo, P. F., Kimmel, J. R., Trimborn, A., Northway, M. J., Jayne, J. T., Aiken, A. C., Gonin, M., Fuhrer, K., Horvath, T., Docherty, K. S., Worsnop, D. R., and Jimenez, J. L.: Field-deployable, high-resolution, time-of-flight aerosol mass spectrometer, Anal. Chem., 78, 8281–8289, doi:10.1021/ac061249n, 2006.

Eddingsaas, N. C., VanderVelde, D. G., and Wennberg, P. O.: Kinetics and products of the acid-catalyzed ring-opening of atmospherically relevant butyl epoxy alcohols, J. Phys. Chem. A, 114, 8106–8113, doi:10.1021/Jp103907c, 2010.

Edney, E. O., Kleindienst, T. E., Jaoui, M., Lewandowski, M., Offenberg, J. H., Wang, W., and Claeys, M.: Formation of 2-methyl tetrols and 2-methylglyceric acid in secondary organic aerosol from laboratory irradiated isoprene/NO_X/SO_2/air mixtures and their detection in ambient $PM_{2.5}$ samples collected in the eastern United States, Atmos. Environ., 39, 5281–5289, doi:10.1016/j.atmosenv.2005.05.031, 2005.

Engelhart, G. J., Asa-Awuku, A., Nenes, A., and Pandis, S. N.: CCN activity and droplet growth kinetics of fresh and aged monoterpene secondary organic aerosol, Atmos. Chem. Phys., 8, 3937–3949, doi:10.5194/acp-8-3937-2008, 2008.

Fountoukis, C. and Nenes, A.: ISORROPIA II: a computationally efficient thermodynamic equilibrium model for K^+–Ca^{2+}–Mg^{2+}–NH_4^+–Na^+–SO_4^{2-}–NO_3^-–Cl^-–H_2O aerosols, Atmos. Chem. Phys., 7, 4639–4659, doi:10.5194/acp-7-4639-2007, 2007.

Fountoukis, C., Nenes, A., Sullivan, A., Weber, R., Van Reken, T., Fischer, M., Matías, E., Moya, M., Farmer, D., and Cohen, R. C.: Thermodynamic characterization of Mexico City aerosol during MILAGRO 2006, Atmos. Chem. Phys., 9, 2141–2156, doi:10.5194/acp-9-2141-2009, 2009.

ACPD
14, 27143–27193, 2014

Gao, S., Keywood, M., Ng, N. L., Surratt, J., Varutbangkul, V., Bahreini, R., Flagan, R. C., and Seinfeld, J. H.: Low-molecular-weight and oligomeric components in secondary organic aerosol from the ozonolysis of cycloalkenes and alpha-pinene, J. Phys. Chem. A, 108, 10147–10164, doi:10.1021/Jp047466e, 2004.

Ghio, A. J., Carraway, M. S., and Madden, M. C.: Composition of air pollution particles and oxidative stress in cells, tissues, and living systems, J. Toxicol. Env. Heal. B, 15, 1–21, doi:10.1080/10937404.2012.632359, 2012.

Hansen, D. A., Edgerton, E. S., Hartsell, B. E., Jansen, J. J., Kandasamy, N., Hidy, G. M., and Blanchard, C. L.: The Southeastern Aerosol Research and Characterization Study: Part 1 – overview, J. Air Waste Manage., 53, 1460–1471, doi:10.1080/10473289.2003.10466318, 2003.

Hansen, D. A., Edgerton, E., Hartsell, B., Jansen, J., Burge, H., Koutrakis, P., Rogers, C., Suh, H., Chow, J., Zielinska, B., McMurry, P., Mulholland, J., Russell, A., and Rasmussen, R.: Air quality measurements for the aerosol research and inhalation epidemiology study, J. Air Waste Manage., 56, 1445–1458, doi:10.1080/10473289.2006.10464549, 2006.

Hennigan, C. J., Bergin, M. H., Dibb, J. E., and Weber, R. J.: Enhanced secondary organic aerosol formation due to water uptake by fine particles, Geophys. Res. Lett., 35, L18801, doi:10.1029/2008gl035046, 2008.

Hennigan, C. J., Izumi, J., Murphy, J. G., Sullivan, A. P., Weber, R. J., Fischer, M. L., Farmer, D. K., Cohen, R. C., and Nenes, A.: A critical evaluation of proxy methods used to estimate the acidity of atmospheric particles, in preparation, Atmos. Chem. Phys., 2014.

Iinuma, Y., Böge, O., Gnauk, T., and Herrmann, H.: Aerosol-chamber study of the α-pinene $/O_3$ reaction: influence of particle acidity on aerosol yields and products, Atmos. Environ., 38, 761–773, doi:10.1016/j.atmosenv.2003.10.015, 2004.

IPCC: Climate Change 2013: The Physical Science Basis, Contribution of Working Group I to the Fifth Assessment Report of the Intergovernmental Panel on Climate Change, Cambridge University Press, Cambridge, UK, New York, NY, USA, 1535 pp., 2013.

Ito, A. and Xu, L.: Response of acid mobilization of iron-containing mineral dust to improvement of air quality projected in the future, Atmos. Chem. Phys., 14, 3441–3459, doi:10.5194/acp-14-3441-2014, 2014.

Jang, M., Czoschke, N. M., Lee, S., and Kamens, R. M.: Heterogeneous atmospheric aerosol production by acid-catalyzed particle-phase reactions, Science, 298, 814–817, doi:10.1126/science.1075798, 2002.

ACPD
14, 27143–27193, 2014

Karambelas, A., Pye, H. O. T., Budisulistiorini, S. H., Surratt, J. D., and Pinder, R. W.: Contribution of isoprene epoxydiol to urban organic aerosol: evidence from modeling and measurements, Environ. Sci. Technol., 1, 278–283, doi:10.1021/ez5001353, 2014.

Kim, J., Yoon, S.-C., Jefferson, A., and Kim, S.-W.: Aerosol hygroscopic properties during Asian dust, pollution, and biomass burning episodes at Gosan, Korea in Apr 2001, Atmos. Environ., 40, 1550–1560, doi:10.1016/j.atmosenv.2005.10.044, 2006.

King, S. M., Rosenoern, T., Shilling, J. E., Chen, Q., and Martin, S. T.: Cloud condensation nucleus activity of secondary organic aerosol particles mixed with sulfate, Geophys. Res. Lett., 34, L24806, doi:10.1029/2007gl030390, 2007.

Kleindienst, T. E., Edney, E. O., Lewandowski, M., Offenberg, J. H., and Jaoui, M.: Secondary organic carbon and aerosol yields from the irradiations of isoprene and α-pinene in the presence of NO_x and SO_2, Environ. Sci. Technol., 40, 3807–3812, doi:10.1021/Es052446r, 2006.

Kotchenruther, R. A. and Hobbs, P. V.: Humidification factors of aerosols from biomass burning in Brazil, J. Geophys. Res., 103, 32081, doi:10.1029/98jd00340, 1998.

Kuwata, M., Zorn, S. R., and Martin, S. T.: Using elemental ratios to predict the density of organic material composed of carbon, hydrogen, and oxygen, Environ. Sci. Technol., 46, 787–794, doi:10.1021/es202525q, 2012.

Lance, S., Nenes, A., Medina, J., and Smith, J. N.: Mapping the operation of the DMT continuous flow CCN counter, Aerosol Sci. Tech., 40, 242–254, doi:10.1080/02786820500543290, 2006.

Liao, H. and Seinfeld, J. H.: Global impacts of gas-phase chemistry-aerosol interactions on direct radiative forcing by anthropogenic aerosols and ozone, J. Geophys. Res.-Atmos., 110, D18208, doi:10.1029/2005jd005907, 2005.

Liu, J., Zhang, X., Parker, E. T., Veres, P. R., Roberts, J. M., de Gouw, J. A., Hayes, P. L., Jimenez, J. L., Murphy, J. G., Ellis, R. A., Huey, L. G., and Weber, R. J.: On the gas-particle partitioning of soluble organic aerosol in two urban atmospheres with contrasting emissions: 2. Gas and particle phase formic acid, J. Geophys. Res., 117, D00V21, doi:10.1029/2012jd017912, 2012.

Magi, B. I. and Hobbs, P. V.: Effects of humidity on aerosols in southern Africa during the biomass burning season, J. Geophys. Res., 108, 8495, doi:10.1029/2002jd002144, 2003.

Malm, W. C. and Day, D. E.: Estimates of aerosol species scattering characteristics as a function of relative humidity, Atmos. Environ., 35, 2845–2860, doi:10.1016/S1352-2310(01)00077-2, 2001.

ACPD
14, 27143–27193, 2014

Meskhidze, N., Chameides, W. L., Nenes, A., and Chen, G.: Iron mobilization in mineral dust: can anthropogenic SO_2 emissions affect ocean productivity?, Geophys. Res. Lett., 30, 2085, doi:10.1029/2003gl018035, 2003.
Meskhidze, N., Chameides, W. L., and Nenes, A.: Dust and pollution: a recipe for enhanced ocean fertilization?, J. Geophys. Res., 110, D03301, doi:10.1029/2004jd005082, 2005.
Mitchell, R. M., Campbell, S. K., Qin, Y., and Gras, J. L.: Performance characteristics of integrating nephelometers in the Australian Outback, J. Atmos. Ocean. Tech., 26, 984–995, doi:10.1175/2008jtecha1187.1, 2009.
Nemesure, S., Wagener, R., and Schwartz, S. E.: Direct shortwave forcing of climate by the anthropogenic sulfate aerosol: sensitivity to particle size, composition, and relative humidity, J. Geophys. Res.-Atmos., 100, 26105–26116, doi:10.1029/95jd02897, 1995.
Nenes, A., Pandis, S. N., and Pilinis, C.: ISORROPIA: a new thermodynamic equilibrium model for multiphase multicomponent inorganic aerosols, Aquat. Geochem., 4, 123–152, doi:10.1023/A:1009604003981, 1998.
Nenes, A., Krom, M. D., Mihalopoulos, N., Van Cappellen, P., Shi, Z., Bougiatioti, A., Zarmpas, P., and Herut, B.: Atmospheric acidification of mineral aerosols: a source of bioavailable phosphorus for the oceans, Atmos. Chem. Phys., 11, 6265–6272, doi:10.5194/acp-11-6265-2011, 2011.
Nguyen, T. K. V., Petters, M. D., Suda, S. R., and Carlton, A. G.: Trends in particle phase liquid water during the Southern Oxidant and Aerosol Study, Atmos. Chem. Phys. Discuss., 14, 7469–7516, doi:10.5194/acpd-14-7469-2014, 2014.
Nowak, J. B., Huey, L. G., Russell, A. G., Tian, D., Neuman, J. A., Orsini, D., Sjostedt, S. J., Sullivan, A. P., Tanner, D. J., Weber, R. J., Nenes, A., Edgerton, E., and Fehsenfeld, F. C.: Analysis of urban gas phase ammonia measurements from the 2002 Atlanta Aerosol Nucleation and Real-Time Characterization Experiment (ANARChE), J. Geophys. Res., 111, D03301, doi:10.1029/2006jd007113, 2006.
Orsini, D. A., Ma, Y., Sullivan, A., Sierau, B., Baumann, K., and Weber, R. J.: Refinements to the particle-into-liquid sampler (PILS) for ground and airborne measurements of water soluble aerosol composition, Atmos. Environ., 37, 1243–1259, doi:10.1016/s1352-2310(02)01015-4, 2003.
Pathak, R. K., Wang, T., Ho, K. F., and Lee, S. C.: Characteristics of summertime $PM_{2.5}$ organic and elemental carbon in four major Chinese cities: implications of

ACPD
14, 27143–27193, 2014

high acidity for water-soluble organic carbon (WSOC), Atmos. Environ., 45, 318–325, doi:10.1016/j.atmosenv.2010.10.021, 2011.
Petters, M. D. and Kreidenweis, S. M.: A single parameter representation of hygroscopic growth and cloud condensation nucleus activity, Atmos. Chem. Phys., 7, 1961–1971, doi:10.5194/acp-7-1961-2007, 2007.
Pilinis, C., Pandis, S. N., and Seinfeld, J. H.: Sensitivity of direct climate forcing by atmospheric aerosols to aerosol-size and composition, J. Geophys. Res.-Atmos., 100, 18739–18754, doi:10.1029/95jd02119, 1995.
Pye, H. O., Pinder, R. W., Piletic, I. R., Xie, Y., Capps, S. L., Lin, Y. H., Surratt, J. D., Zhang, Z., Gold, A., Luecken, D. J., Hutzell, W. T., Jaoui, M., Offenberg, J. H., Kleindienst, T. E., Lewandowski, M., and Edney, E. O.: Epoxide pathways improve model predictions of isoprene markers and reveal key role of acidity in aerosol formation, Environ. Sci. Technol., 47, 11056–11064, doi:10.1021/es402106h, 2013.
Roberts, G. C. and Nenes, A.: A continuous-flow streamwise thermal-gradient CCN chamber for atmospheric measurements, Aerosol Sci. Tech., 39, 206–221, doi:10.1080/027868290913988, 2005.
Seinfeld, J. H. and Pandis, S. N.: Atmospheric Chemistry and Physics: From Air Pollution to Climate Change 2nd Edition, John Wiley & Sons, Inc., Hoboken, New Jersey, 2006.
Sheridan, P. J., Jefferson, A., and Ogren, J. A.: Spatial variability of submicrometer aerosol radiative properties over the Indian Ocean during INDOEX, J. Geophys. Res., 107, 8011, doi:10.1029/2000jd000166, 2002.
Sloane, C. S., Watson, J., Chow, J., Pritchett, L., and Richards, L. W.: Size-segregated fine particle measurements by chemical-species and their impact on visibility impairment in Denver, Atmos. Environ. A-Gen., 25, 1013–1024, doi:10.1016/0960-1686(91)90143-U, 1991.
Sorooshian, A., Hersey, S., Brechtel, F. J., Corless, A., Flagan, R. C., and Seinfeld, J. H.: Rapid, size-resolved aerosol hygroscopic growth measurements: Differential Aerosol Sizing and Hygroscopicity Spectrometer Probe (DASH-SP), Aerosol Sci. Tech., 42, 445–464, doi:10.1080/02786820802178506, 2008.
Stein, S. W., Turpin, B. J., Cai, X. P., Huang, C. P. F., and Mcmurry, P. H.: Measurements of relative humidity-dependent bounce and density for atmospheric particles using the DMA-Impactor technique, Atmos. Environ., 28, 1739–1746, doi:10.1016/1352-2310(94)90136-8, 1994.

ACPD
14, 27143–27193, 2014

Surratt, J. D., Lewandowski, M., Offenberg, J. H., Jaoui, M., Kleindienst, T. E., Edney, E. O., and Seinfeld, J. H.: Effect of acidity on secondary organic aerosol formation from isoprene, Environ. Sci. Technol., 41, 5363–5369, 2007.

Surratt, J. D., Chan, A. W., Eddingsaas, N. C., Chan, M., Loza, C. L., Kwan, A. J., Hersey, S. P., Flagan, R. C., Wennberg, P. O., and Seinfeld, J. H.: Reactive intermediates revealed in secondary organic aerosol formation from isoprene, P. Natl. Acad. Sci. USA, 107, 6640–6645, doi:10.1073/pnas.0911114107, 2010.

Tang, I. N.: Phase transformation and growth of aerosol particles composed of mixed salts, J. Aerosol Sci., 7, 361–371, doi:10.1016/0021-8502(76)90022-7, 1976.

Tang, I. N. and Munkelwitz, H. R.: Composition and temperature-dependence of the deliquescence properties of hygroscopic aerosols, Atmos. Environ. A-Gen., 27, 467–473, doi:10.1016/0960-1686(93)90204-C, 1993.

Tanner, R. L., Olszyna, K. J., Edgerton, E. S., Knipping, E., and Shaw, S. L.: Searching for evidence of acid-catalyzed enhancement of secondary organic aerosol formation using ambient aerosol data, Atmos. Environ., 43, 3440–3444, doi:10.1016/j.atmosenv.2009.03.045, 2009.

Tolocka, M. P., Jang, M., Ginter, J. M., Cox, F. J., Kamens, R. M., and Johnston, M. V.: Formation of oligomers in secondary organic aerosol, Environ. Sci. Technol., 38, 1428–1434, 2004.

Turpin, B. J. and Lim, H.-J.: Species contributions to $PM_{2.5}$ mass concentrations: revisiting common assumptions for estimating organic mass, Aerosol Sci. Tech., 35, 602–610, doi:10.1080/02786820119445, 2001.

Verma, V., Fang, T., Guo, H., King, L., Bates, J. T., Peltier, R. E., Edgerton, E., Russell, A. J., and Weber, R. J.: Reactive oxygen species associated with water-soluble $PM_{2.5}$ in the southeastern United States: spatiotemporal trends and source apportionment, Atmos. Chem. Phys. Discuss., 14, 19625–19672, doi:10.5194/acpd-14-19625-2014, 2014.

Wexler, A. S. and Seinfeld, J. H.: Second-generation inorganic aerosol model, Atmos. Environ. A-Gen., 25, 2731–2748, doi:10.1016/0960-1686(91)90203-J, 1991.

Xu, L., Guo, H., Boyd, C. M., Klein, M., Bougiatioti, A., Cerully, K. M., Hite, J. R., Isaacman-VanWertz, G., Kreisberg, N. M., Knote, C., Olson, K., Koss, A., Goldstein, A. H., Hering, S. V., Gouw, J. D., Baumann, K., Lee, S. H., Nenes, A., Weber, R. J., and Ng, N. L.: Effects of Anthropogenic Emissions on Aerosol Formation from Isoprene and Monoterpenes in the Southeastern United States, in review, 2014.

Yin, L., Niu, Z., Chen, X., Chen, J., Zhang, F., and Xu, L.: Characteristics of water-soluble inorganic ions in $PM_{2.5}$ and $PM_{2.5-10}$ in the coastal urban agglomeration along the Western

ACPD
14, 27143–27193, 2014

Taiwan Strait Region, China, Environ. Sci. Pollut. R., 21, 5141–5156, doi:10.1007/s11356-013-2134-7, 2014.

You, Y., Renbaum-Wolff, L., Carreras-Sospedra, M., Hanna, S. J., Hiranuma, N., Kamal, S., Smith, M. L., Zhang, X., Weber, R. J., Shilling, J. E., Dabdub, D., Martin, S. T., and Bertram, A. K.: Images reveal that atmospheric particles can undergo liquid–liquid phase separations, P. Natl. Acad. Sci. USA, 109, 13188–13193, doi:10.1073/pnas.1206414109, 2012.

You, Y., Kanawade, V. P., de Gouw, J. A., Guenther, A. B., Madronich, S., Sierra-Hernández, M. R., Lawler, M., Smith, J. N., Takahama, S., Ruggeri, G., Koss, A., Olson, K., Baumann, K., Weber, R. J., Nenes, A., Guo, H., Edgerton, E. S., Porcelli, L., Brune, W. H., Goldstein, A. H., and Lee, S.-H.: Atmospheric amines and ammonia measured with a Chemical Ionization Mass Spectrometer (CIMS), Atmos. Chem. Phys. Discuss., 14, 16411–16450, doi:10.5194/acpd-14-16411-2014, 2014.

Zhang, X., Liu, Z., Hecobian, A., Zheng, M., Frank, N. H., Edgerton, E. S., and Weber, R. J.: Spatial and seasonal variations of fine particle water-soluble organic carbon (WSOC) over the southeastern United States: implications for secondary organic aerosol formation, Atmos. Chem. Phys., 12, 6593–6607, doi:10.5194/acp-12-6593-2012, 2012.

ACPD
14, 27143–27193, 2014

Table 1. Deployment status of instruments at various sites. All the listed instruments or probes were operated at CTR for SOAS.

Site	Period (mm yyyy)	PILS-IC	AMS	CCNc	Nephelometer	TEOM	RH and *T*
JST	May and Nov 2012	NO	YES	NO	NO	YES	YES
YRK	Jul and Dec 2012	NO	YES	NO	NO	YES	YES
GIT	Jul–Aug 2012	NO	YES	NO	NO	YES	YES
RS	Sep 2012	NO	YES	NO	NO	YES	YES
CTR	Jun–Jul 2013	YES	YES	YES	YES	YES	YES

ACPD
14, 27143–27193, 2014

Table 2. Sensitivity of H^+ to ions from ANISORROPIA (2nd row) and contribution of uncertainty. Uncertainties of inorganic ions ($\frac{\delta_{Ion}}{Ion}$) are calculated based on a combination of PILS-IC instrumental relative uncertainties (IC uncertainty, referred to as $\frac{\delta_{ion,\,IC}}{Ion}$, all estimated to be 15 %) and the difference between PILS-IC and AMS ($\frac{\delta_{Ion,IC-AMS}}{Ion}$, defined as the (slope – 1) in Fig. 1) (3rd row), where $\frac{\delta_{Ion}}{Ion} = \sqrt{(\frac{\delta_{ion,\,IC}}{Ion})^2 + (\frac{\delta_{Ion,IC-AMS}}{Ion})^2}$ (4th row). Contribution of uncertainty is the ratio of ion uncertainty over H^+ uncertainty ($\frac{\delta_{H^+}}{H^+}$, calculated to be 14 % in Eq. 8) (5th row).

PILS-IC ion concentration, $\mu g\,m^{-3}$ (mean ± SD)	SO_4 1.73 ± 1.21	NH_4 0.46 ± 0.34	Na 0.03 ± 0.07	NO_3 0.08 ± 0.08	Cl 0.02 ± 0.03
H^+ Sensitivity (mean ± SD)	$\left\lvert\frac{\partial H^+}{\partial SO_4}\right\rvert$ 0.51 ± 0.34	$\left\lvert\frac{\partial H^+}{\partial NH_4}\right\rvert$ 0.32 ± 0.31	$\left\lvert\frac{\partial H^+}{\partial Na}\right\rvert$ 0.19 ± 0.27	$\left\lvert\frac{\partial H^+}{\partial NO_3}\right\rvert$ 0.002 ± 0.007	$\left\lvert\frac{\partial H^+}{\partial Cl}\right\rvert$ 0.000 ± 0
$\frac{\delta_{Ion,\,IC-AMS}}{Ion}$	$\frac{\delta_{SO_4,\,IC-AMS}}{SO_4}$ 20.5 %	$\frac{\delta_{NH_4,\,IC-AMS}}{NH_4}$ 1.5 %	$\frac{\delta_{Na,\,IC-AMS}}{Na}$ N/A[a]	$\frac{\delta_{NO_3,\,IC-AMS}}{NO_3}$ [b]	$\frac{\delta_{Cl,\,IC-AMS}}{Cl}$ [b]
$\frac{\delta_{Ion}}{Ion}$	$\frac{\delta_{SO_4}}{SO_4}$ 25.4 %	$\frac{\delta_{NH_4}}{NH_4}$ 15.1 %	$\frac{\delta_{Na}}{Na}$ 15 %	$\frac{\delta_{NO_3}}{NO_3}$ 15 %	$\frac{\delta_{Cl}}{Cl}$ 15 %
Contribution to H^+ uncertainty	$\frac{\left\lvert\frac{\partial H^+}{\partial SO_4}\right\rvert \cdot \frac{\delta_{SO_4}}{SO_4}}{\frac{\delta_{H^+}}{H^+}}$ 0.93	$\frac{\left\lvert\frac{\partial H^+}{\partial NH_4}\right\rvert \cdot \frac{\delta_{NH_4}}{NH_4}}{\frac{\delta_{H^+}}{H^+}}$ 0.35	$\frac{\left\lvert\frac{\partial H^+}{\partial Na}\right\rvert \cdot \frac{\delta_{Na}}{Na}}{\frac{\delta_{H^+}}{H^+}}$ 0.20	$\frac{\left\lvert\frac{\partial H^+}{\partial NO_3}\right\rvert \cdot \frac{\delta_{NO_3}}{NO_3}}{\frac{\delta_{H^+}}{H^+}}$ 0.002	$\frac{\left\lvert\frac{\partial H^+}{\partial Cl}\right\rvert \cdot \frac{\delta_{Cl}}{Cl}}{\frac{\delta_{H^+}}{H^+}}$ 0.000

[a] Na is not measured by AMS.

[b] $\left\lvert\frac{\partial H^+}{\partial NO_3}\right\rvert$ and $\left\lvert\frac{\partial H^+}{\partial Cl}\right\rvert$ are less than 1 % of the other H^+ sensitivities, and the loadings of NO_3 and Cl are less than 5 % of the total inorganic ion mass. As a result, their contributions to H^+ uncertainty are negligible.

ACPD
14, 27143–27193, 2014

Table 3. Water and pH prediction for SCAPE sites. Means and SDs are listed, if not specified. Total ion concentration is counted as the sum of AMS inorganics (3rd row). $\varepsilon(W_o)$ is the mass fraction of W_o (5th row).

	JST May 2012	YRK Jul 2012	GIT Aug 2012	RS Sep 2012	JST Nov 2012	YRK Dec 2012
RH, % T, °C	67 ± 19 23.1 ± 4.3	66 ± 21 27.7 ± 4.4	71 ± 17 26.3 ± 3.5	72 ± 20 21.4 ± 3.8	63 ± 19 11.5 ± 4.8	73 ± 21 9.8 ± 5.2
Total ion concentration, $\mu g\,m^{-3}$	4.1 ± 2.1	4.5 ± 2.2	5.3 ± 2.6	4.1 ± 2.7	3.6 ± 2.1	2.3 ± 1.8
$\frac{\delta_{pH}}{pH}$ from 1.10 RH Total $\frac{\delta_{pH}}{pH}$	22.3 % 23.9 %	21.4 % 23.0 %	48.3 % 49.0 %	22.1 % 23.7 %	2.5 % 8.8 %	1.4 % 8.6 %
$\varepsilon(W_o)$, %	34 ± 11	37 ± 8	33 ± 10	38 ± 11	39 ± 16	29 ± 15
LWC, $\mu g\,m^{-3}$ pH*	5.98 ± 6.28 1.3 ± 0.7	8.14 ± 8.47 1.1 ± 0.6	8.41 ± 7.67 1.1 ± 0.4	7.81 ± 9.23 1.3 ± 0.7	5.88 ± 8.69 2.2 ± 0.9	3.24 ± 3.46 1.8 ± 1.0
LWC, $\mu g\,m^{-3}$ (median) pH* (median)	3.74 ± 6.28 1.2 ± 0.7	5.29 ± 8.47 1.0 ± 0.6	6.06 ± 7.67 1.0 ± 0.4	4.31 ± 9.23 1.2 ± 0.7	2.14 ± 8.69 2.3 ± 0.9	2.02 ± 3.46 1.8 ± 1.0

* A bias correction of 1 pH unit is applied due to not considering ammonia partitioning.

ACPD
14, 27143–27193, 2014

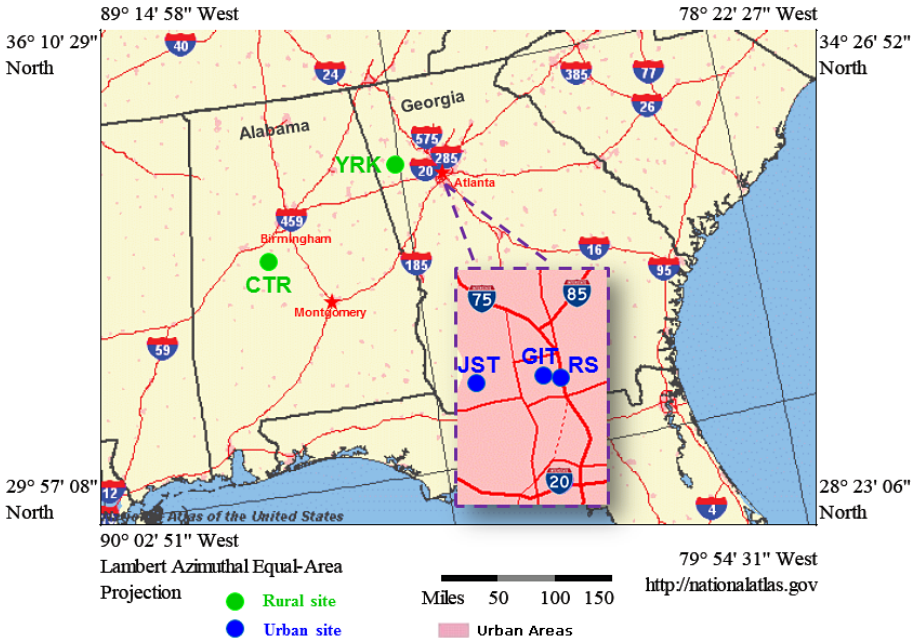

Figure 1. Sampling sites in the southeastern USA, consisting of two rural and three urban sites.

ACPD
14, 27143–27193, 2014

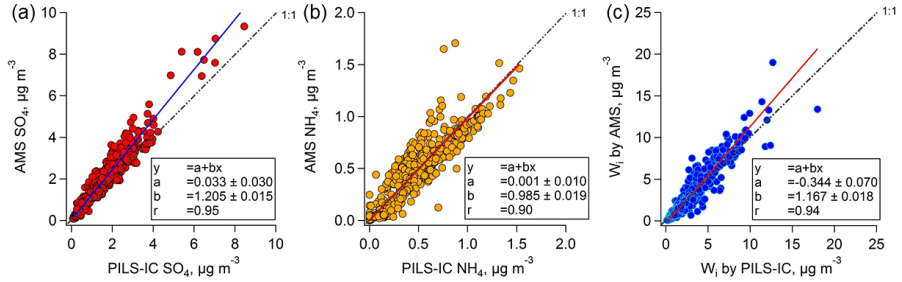

Figure 2. Comparisons of PM_1 AMS sulfate, ammonium to PM_1 and $PM_{2.5}$ PILS-IC (i.e. complete SOAS study) and predicted W_i. Orthogonal distance regression (ODR) fits were applied.

ACPD
14, 27143–27193, 2014

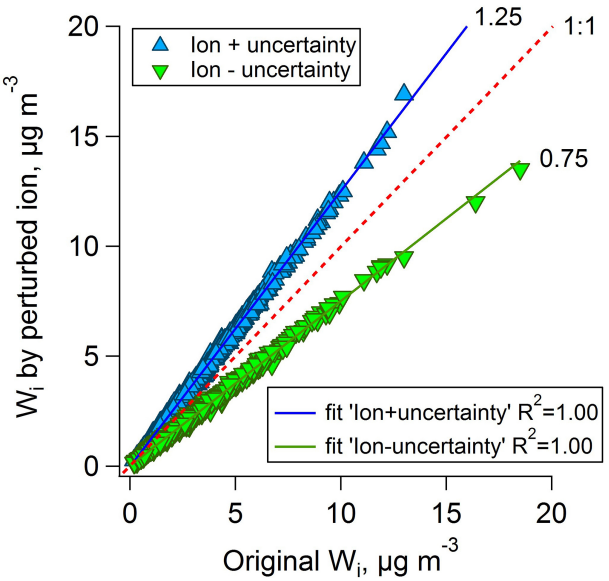

Figure 3. W_i based on artificially perturbed ion data at upper and lower uncertainty limits. The slopes indicate W_i uncertainty caused by ions.

ACPD
14, 27143–27193, 2014

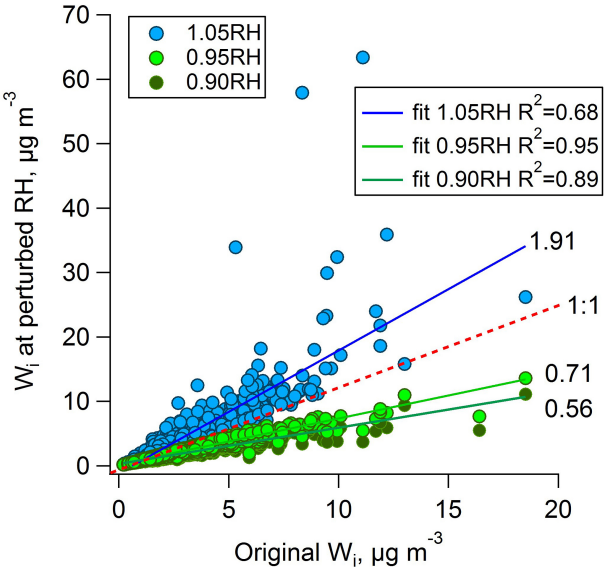

Figure 4. W_i based on artificially perturbed RH at upper and lower uncertainty limits. 1.10 RH (i.e., RH increased by 10 %) is not plotted because it results in much larger W_i than the rest. Slopes and R^2 indicate corresponding W_i uncertainty caused by variability (uncertainty) in RH.

ACPD
14, 27143–27193, 2014

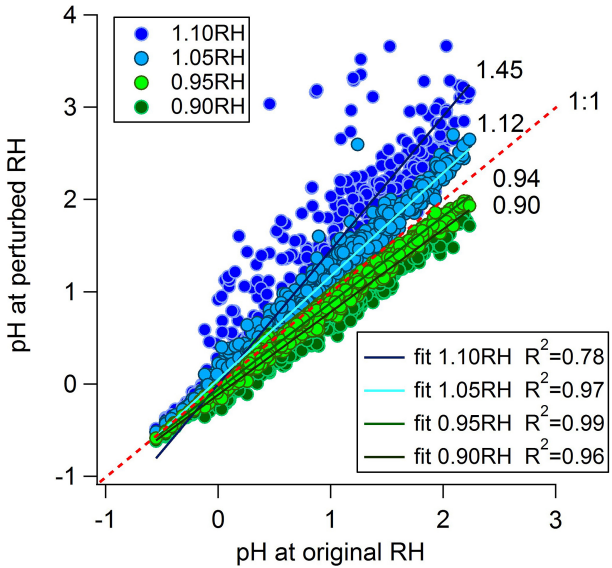

Figure 5. pH predictions by perturbed RH. W_i, W_o, and H^+_{air} were recalculated based on ±5 and ±10 % original RH to investigate pH uncertainty. The slopes and R^2 indicate pH uncertainty caused by RH.

ACPD
14, 27143–27193, 2014

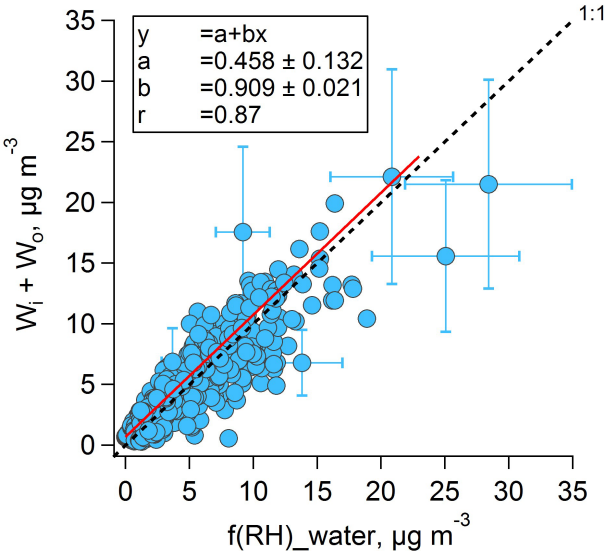

Figure 6. Comparison between total predicted and measured water by nephelometers based on hourly averaged data at CTR (SOAS). An ODR fit was applied. Error bars for selected points are shown.

ACPD
14, 27143–27193, 2014

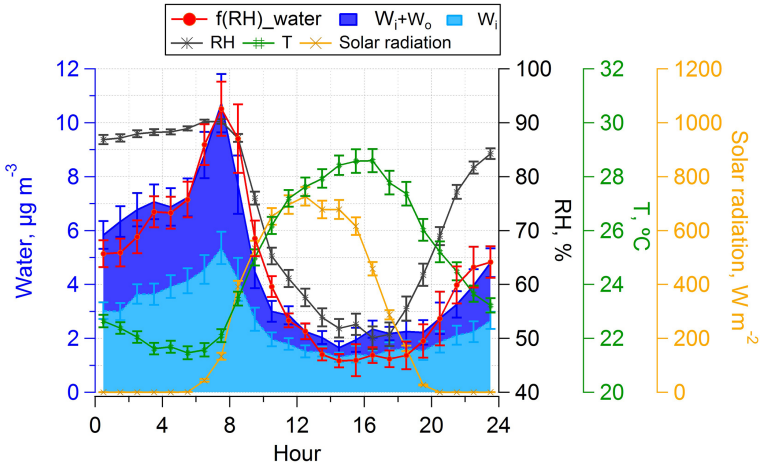

Figure 7. CTR (SOAS) diurnal profiles of predicted and measured water, measured RH, *T*, and solar radiation. Median hourly averages and standard error plotted as error bars at local hour are shown.

ACPD
14, 27143–27193, 2014

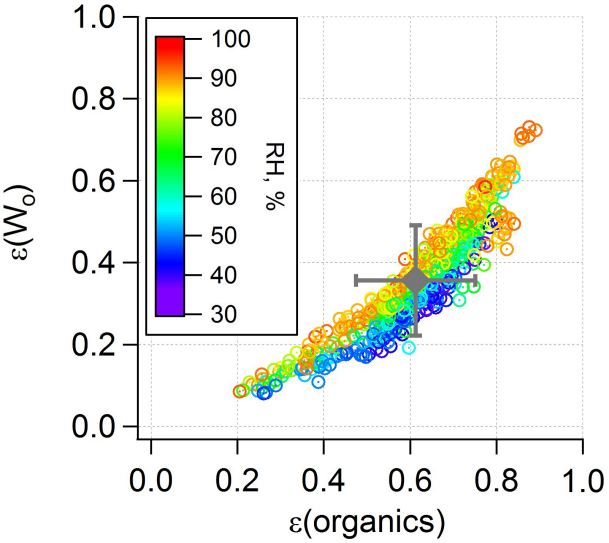

Figure 8. W_o fraction plotted with organic mass fraction at CTR (SOAS). Overall study mean and SD is also shown. $\varepsilon_{\text{Organic}} = 61 \pm 14\,\%$ and $\varepsilon_{W_o} = 36 \pm 14\,\%$.

ACPD
14, 27143–27193, 2014

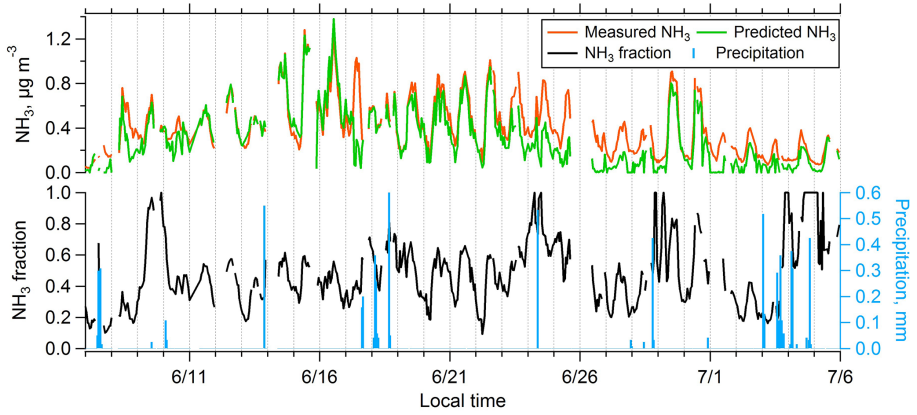

Figure 9. CTR (SOAS) time series of hourly averaged measured $NH_{3(g)}$, predicted $NH_{3(g)}$, $NH_{3(g)}$ fraction (i.e., measured $NH_{3(g)}/(NH_{3(g)} + NH_{4(p)})$) and precipitation.

ACPD
14, 27143–27193, 2014

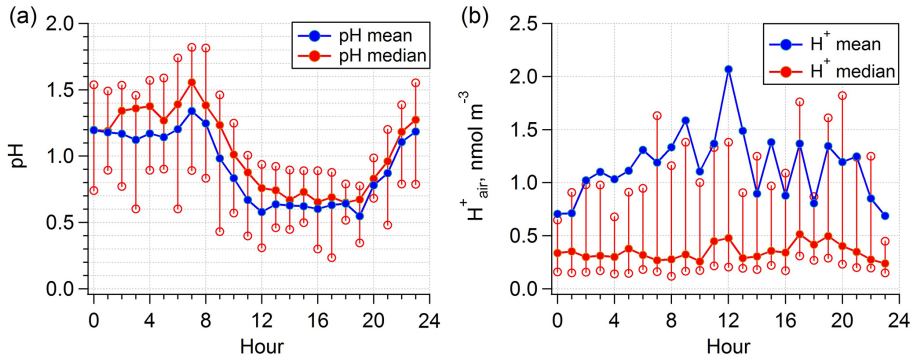

Figure 10. CTR (SOAS) diurnal patterns of calculated pH based on total predicted water (W_i + W_o) and H^+_{air} predicted by ISORROPIA-II. Mean and median values are shown, together with 25 % and 75 quantiles marked as non-filled circles.

ACPD
14, 27143–27193, 2014

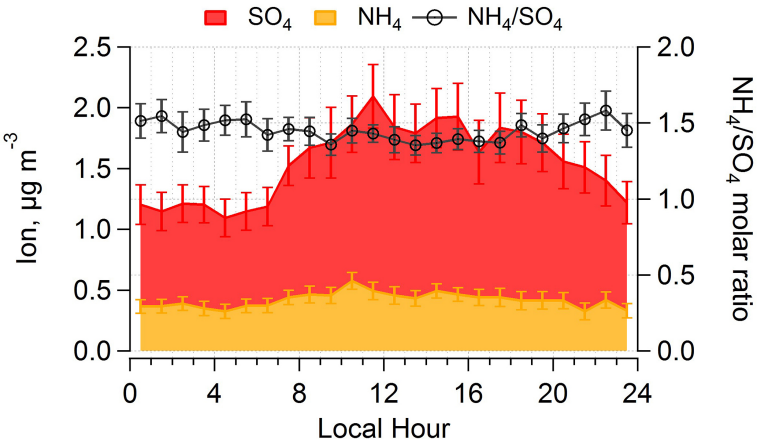

Figure 11. CTR (SOAS) diurnal patterns of PILS-IC NH_4 and SO_4, and the molar ratio. Median hourly averages and standard error bars at local hours are plotted.

ACPD
14, 27143–27193, 2014

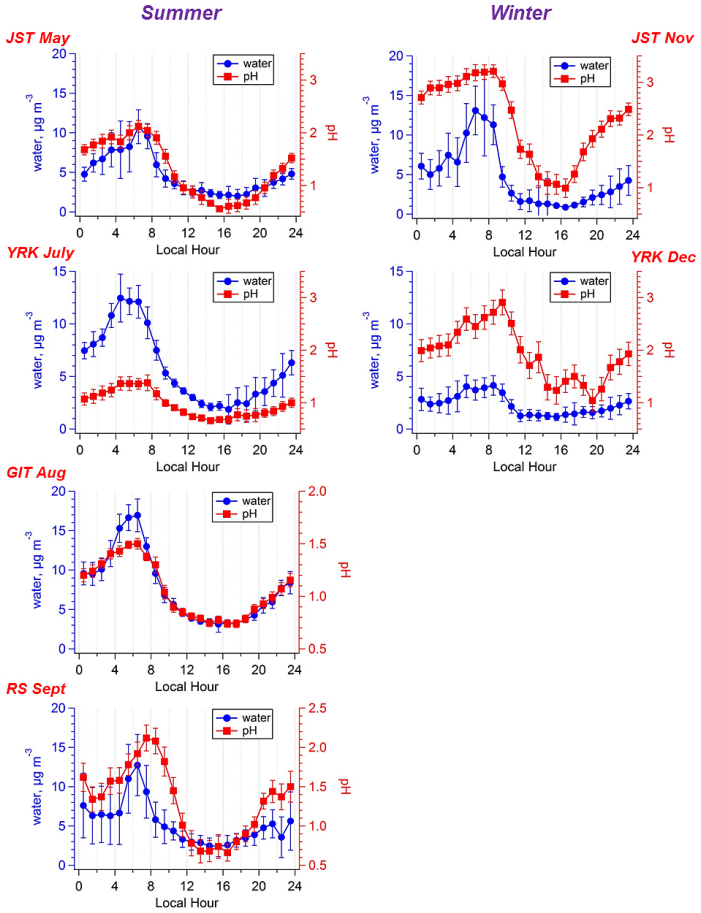

Figure 12. LWC and pH diurnal variation at SCAPE sites: comparison between summer and winter. Median hourly averages and standard error bars at local hour are plotted. A bias correction of 1 pH unit is applied due to not considering ammonia partitioning.

ACPD
14, 27143–27193, 2014

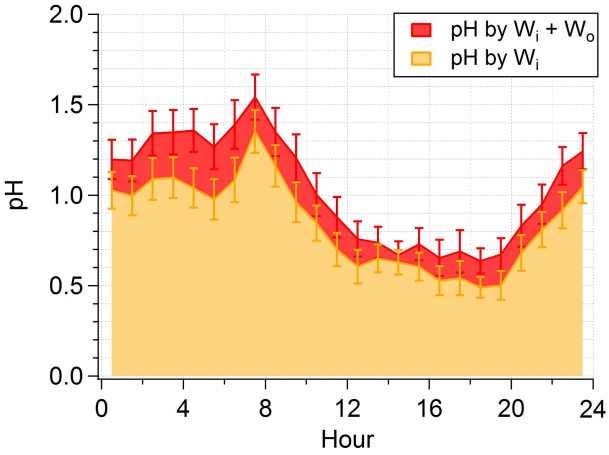

Figure 13. CTR (SOAS) pH diurnal profiles based on total predicted water and W_i, respectively. Median hourly averages and standard error bars at local hour are plotted.

ACPD
14, 27143–27193, 2014

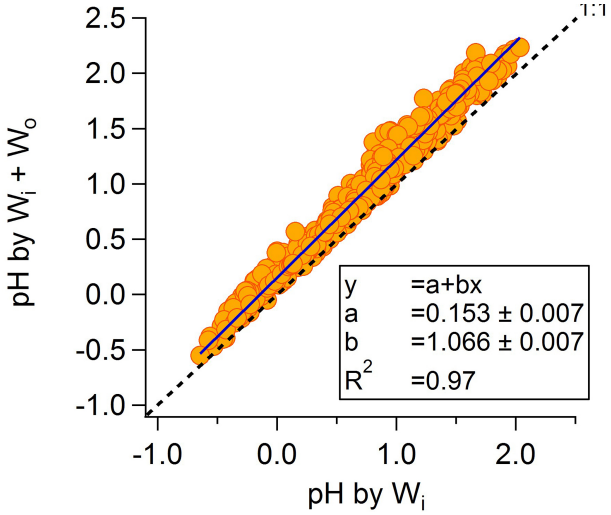

Figure 14. Comparison between pH based on W_i and pH based on total predicted water at CTR (SOAS). An ODR fit was applied.

ACPD
14, 27143–27193, 2014